

RESEARCH ARTICLE

New Safety Feedback Control Design to Guarantee Adequate Frequency Performance in Microgrids

Fatima Taousser¹ D | Samaneh Morovati² | Yichen Zhang³ D | Seddik M. Djouadi¹ | Kevin Tomsovic¹ | Mohammed Olama⁴

¹Department of Electrical Engineering and Computer Science, The University of Tennessee, Knoxville, Tennessee, USA | ²Quanta Technology, LLC, Quanta Technology, LLC, Raleigh, North Carolina, USA | ³Department of Electrical Engineering, University of Texas at Arlington, Arlington, Texas, USA | ⁴Computational Sciences and Engineering Division, Oak Ridge National Laboratory, Oak Ridge, Tennessee, USA

Correspondence: Fatima Taousser (ftaousse@utk.edu)

Received: 30 April 2023 | Revised: 9 November 2023 | Accepted: 18 September 2024

Funding: This work has been supported by the National Science Foundation and the Department of Energy under NSF Award Number EECS-2208218, the Engineering Research Center Program of the National Science Foundation and the Department of Energy under NSF Award Number EEC-1041877. This manuscript has been authored by UT-Battelle, LLC, under contract DE-AO05-00OR22725 with the US Department of Energy (DOE). The US government retains and the publisher, by accepting the article for publication, acknowledges that the US government retains a nonexclusive, paid-up, irrevocable, worldwide license to publish or reproduce the published form of this manuscript, or allow others to do, for US government purposes. DOE Public Access Plan (http://www.energy.gov/doe-public-access-plan).

Keywords: barrier function | safety property | stability analysis | switched systems | wind turbine generator

ABSTRACT

Safety analysis of power systems is concerned with the system's ability to maintain critical variables within specified limits following a disturbance. Frequency control adequacy has become increasingly important as the system inertia decreases due to the increase in renewable energy penetration. Various controllers for inverters have been proposed to improve the system frequency response and few are capable to ensure the safety of the response. In this article, a diesel-wind energy system is considered and modeled as a switching system between normal, faulted, and post-fault modes. A safety feedback controller is designed as a supplementary signal for a wind turbine generator such that the speed of the diesel generator stays within a permissible range in the presence of a finite energy disturbance. Numerical results on the modified 33-bus microgrid system obtained of the proposed novel approach indicate that the suggested control configuration can guarantee adequate frequency response without excessive conservativeness.

1 | Introduction

Renewable resources have been providing an increasing portion of the total generation in power systems, particularly in islanded microgrids. Since most renewable resources are not electromechanically coupled to the microgrid, the replacement of traditional synchronous generators results in a decrease of system inertia and inadequacy of frequency response [1, 2]. Large transients in frequency can trigger unnecessary relay actions even though the system has adequate capacity to reach

a viable steady-state [3]. Therefore, maintaining the system frequency within permissible ranges is critical to reliable electricity delivery [4], especially in the islanded mode of operation for microgrids.

Currently, most converters in renewable resources have the capability to provide grid supportive controls (GSCs), although they may not be commonly deployed. These controls can be divided into two categories. The first and most widely studied methods are to provide an additional signal. On the one

© 2024 John Wiley & Sons Ltd.

hand, this signal can be generated as a function of the grid frequency, including grid frequency deviation to emulate primary response [5–8], rate of change of frequency to emulate inertial response [9–12], and a mix of both [13–17]. On the other hand, a pre-specified reference signal (referred to as the power surge control) to the torque/power [18–21] or a speed reference value to be tracked [14] is required. These methods can be referred to as supplementary-signal based methods. The second category uses power electronic control, either in the phase-lock loop (PLL) [22] or the active power controller [23, 24], to mimic the power-angle relation of traditional synchronous generators. Consequently, the angle used by the Park's transformation for synchronization is no longer obtained through the vector alignment, but it is determined using the swing dynamics.

There are multiple goals for such controls. The simpler objective is to improve the frequency response under the capacity limits of the resources, which most microgrid supportive controllers are designed for. A more challenging control task is to provide guaranteed control specifications, for example, emulating a given inertia constant or ensuring an acceptable frequency nadir given a pre-defined disturbance set. The latter objective is more challenging and only a few researchers have tackled it. In [3], energy storage systems are used to avoid unnecessary under-frequency load shedding (UFLS), where a composite model of system frequency response (SFR) is built to evaluate the frequency performance with support. In [8], a safety supervisory control is designed to switch the mode of a wind turbine generator between the maximum power point tracking (MPPT) and GSC mode to ensure frequency adequacy. But, this structure relies on a fixed GSC and thus, provides guarantees under a limited range of disturbances. In [25], a commitment strategy for interruptible loads to ensure adequate response is proposed. However, the frequency nadir information under different commitments of interruptible loads needs to be obtained via simulation and sensitivity prediction. In [26], the available time remaining for resources to take actions to guarantee a bounded frequency response given a disturbance is estimated as a function of local inertia. However, the impact of the supportive control on this reaction time is not assessed. This could lead to inadequate responses when the supportive control is not strong enough to alter the rate of change of frequency. As one can see, most works that tackle the challenge of performance guarantees are based on the assumption of a fixed controller.

Motivated by such issues, this article investigates supportive feedback control design to guarantee system frequency performance safety when a disturbance occurs in an islanded microgrid. The safety region is given and determined by a barrier function as a metric, such that when the perturbed system reaches the boundary of the region, which has to be determined, the feedback controller will be activated to ensure the system frequency remains inside the safety region.

The contribution of this article is two-fold as outlined:

 First, this work proposes a control design mechanism to ensure trajectory performance in an islanded microgird. We give a necessary and sufficient condition of the existence of a controller that depends on the barrier function chosen and the energy of the perturbation. A linearized reduced order model of the augmented plant is used to drive the theoretic approach, and the obtained controller is tested on a modified 33 bus based microgrid in Simulink environment for validation.

• The second contribution is the estimation of the critical time available to apply the control law in order to prevent the frequency from reaching the unsafe region.

Note that, in this article we are considering that the perturbation will occur during a certain period and will be cleared after some time. The main problem here is not to design a feedback controller that will reject or attenuate the disturbance, as it has been studied in most of the papers in the literature on disturbances in linear systems (see [27–31]), but to design a supportive feedback controller to improve the frequency response by considering its reaction time.

The article is organized as follows. Section 2 recalls useful concepts on safety and control barrier function to guarantee frequency performance. Section 3 describes the power system and the safety problem of the frequency response. In Section 4, the required conditions are derived to construct a control feedback that assures the safety of the system in the presence of a finite energy disturbance with respect to a barrier function and determine the critical time when the controller needs to be applied to ensure the safety of the frequency. Illustrative simulations are given in Section 5 to show the effectiveness of the proposed method.

2 | Preliminaries

Safety¹ is the property that all trajectories of a system stay within given bounded regions. Consider the following nonlinear dynamical system

$$\dot{x}(t) = f(x(t), d(t)) \tag{1}$$

where $x(t) \in \mathbb{R}^n$ is the state vector and $d(t) \in \mathbb{R}^m$ is the disturbance. The notion of safety is made concrete by the following definition.

Definition 1. Given a set of admissible states $\mathbb{X} \subset \mathbb{R}^n$, a set of initial states $\mathcal{X}_0 \subset \mathbb{X}$, a set of unsafe states $\mathcal{X}_u \subset \mathbb{X}$, and a set of bounded disturbances $\mathcal{D} \subset \mathbb{R}^m$. Let $\mathbb{X}(\mathcal{X}_0, t, d(t))$ be the set of trajectories initialized in \mathcal{X}_0 . The safety property holds for the nonlinear system (1) if there exists no time $T \geq 0$ and no bounded disturbance $d: [0,T] \to \mathcal{D}$, such that $\mathbb{X}(\mathcal{X}_0,t,d(t)) \cap \mathcal{X}_u \neq \emptyset$, $\forall t \in [0,T]$.

The Safety property can be verified using a function of state, termed barrier certificate, which is used to certify that all trajectories of the system starting from a given initial set do not enter an unsafe region.

Lemma 1. ([32]). Given a nonlinear system $\dot{x} = f(x,d), x \in \mathbb{X} \subset \mathbb{R}^n, d \in \mathcal{D} \subset \mathbb{R}^m$, with $f \in C(\mathbb{X} \times \mathcal{D}, \mathbb{R}^n)$ (the space of continuous functions). Suppose there exists a differentiable function $B : \mathbb{R}^n \to \mathbb{R}$ satisfying (2-4) for the given sets \mathcal{X}_0 and \mathcal{X}_u ,

$$B(x) \le 0 \qquad \forall x \in \mathcal{X}_0 \tag{2}$$

$$B(x) > 0 \qquad \forall x \in \mathcal{X}_{u} \tag{3}$$

$$\frac{\partial B}{\partial x}f(x,d) \le 0 \qquad \forall (x,d) \in \mathbb{X} \times \mathcal{D} \tag{4}$$

Then the safety property holds (for proof see [32]).

The function B is termed a barrier function for the given system. The level curve B(x)=0, called the barrier certificate, separates the safe and unsafe regions. By the above conditions, this curve constitutes a barrier, such that, the trajectories that start from \mathcal{X}_0 cannot cross toward the unsafe set \mathcal{X}_u . Usually, the set of unsafe states \mathcal{X}_u is given by some physical constraints on the system states, for example, UFLS threshold.

To introduce the main result, we review some necessary algebraic tools. For a matrix $M \in \mathbb{C}^{n \times m}$ with rank r < n, let $M^{\perp} \in \mathbb{C}^{(n-r) \times n}$ be any matrix such that $M^{\perp}M = 0$ and $M^{\perp}(M^{\perp})^* > 0$ (which can be computed using the singular value decomposition), where M^* is the complex conjugate transpose of M. Note that such a matrix M^{\perp} exists if and only if M has linearly dependent rows r < n (see [33] for more details).

Theorem 1. ([33]). Let the matrices $B \in \mathbb{C}^{n \times m}$ and $Q = Q^* \in \mathbb{C}^{n \times n}$ be given. The following statements are equivalent.

i. There exists a matrix X satisfying

$$BX + (BX)^* + O < 0$$

ii. The following condition holds

$$B^{\perp}OB^{\perp*} < 0$$
 or $BB^* > 0$

Suppose the above statements hold and further assume that $B^*B > 0$. Then all matrices X in statement (i) are given by

$$X = -\gamma B^* + \sqrt{\gamma} L \Omega^{\frac{1}{2}} \tag{5}$$

where L is any matrix such that ||L|| < 1 and $\gamma > 0$ is any scalar such that $\Omega = (\gamma BB^* - Q) > 0$.

Note that, the equivalence between statements (i) and (ii) is known as *the elimination lemma* (see [34, 35] for the proof).

Lemma 2. ([36]). For any positive definite matrix M > 0, a scalar $\delta > 0$ and a vector function $w : [0, \delta] \to \mathbb{R}^n$, then the following inequality holds:

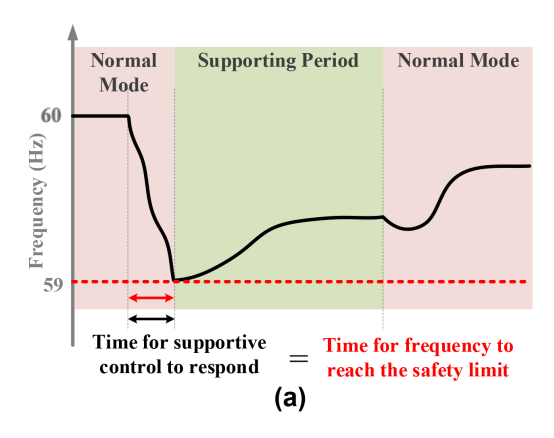
$$\left(\int_{0}^{\delta} w(s)ds\right)^{T} M\left(\int_{0}^{\delta} w(s)ds\right) \le \delta \int_{0}^{\delta} w^{T}(s) Mw(s)ds \qquad (6)$$

3 | Problem Statement

When power systems undergo a sudden generation-load imbalance, synchronous generators will provide an immediate inertial response. The underlying physical process of the inertial responses is that the kinetic energy stored in the rotating mass of synchronous generators is released and converted into electric energy due to the electromagnetic coupling between synchronous generators and the electric grid. In turn, the energy conversion leads to the decline of generator rotational speed, and therefore system frequency [37]. This process is governed by the swing equation below

$$\Delta \dot{\omega} = \frac{1}{2H} \Delta P \tag{7}$$

where ΔP denotes the power imbalance with a negative sign denoting generation shortage and a positive sign denoting generation surplus. If the converted electric energy is not adequate to eliminate the power imbalance, the system frequency will continue declining and exceed the dead-band of primary frequency control, activating it. The primary frequency control measures the frequency deviation and sends a proportional signal to the turbine to increase the mechanical power input, thus eliminating any power imbalance. During the entire process, (7) indicates that as long as there still exists a generation shortage, that is, negative ΔP , the frequency will continue declining and more quickly when the inertia constant H is smaller. Therefore, the goal of GSCs is to relieve the power imbalance. More importantly, since most renewable resources are operated under the MPPT mode in normal operations, the switching time into GSCs is one dominant factor to ensure a safe frequency response. It is important to investigate the critical switching time; the maximum allowable time to switch to the supportive control mode to ensure the safety of the frequency response [38]. Regarding the critical switching time, two circumstances may occur, as illustrated in Figure 1. Figure 1a



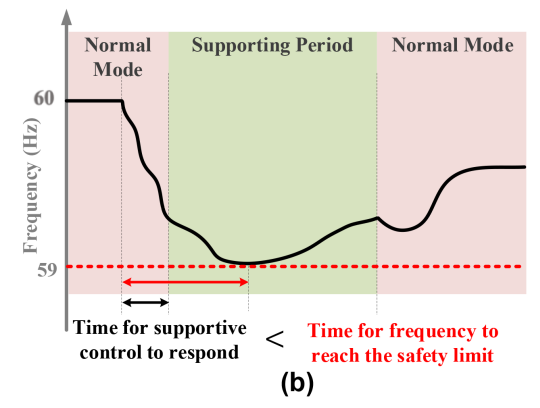


FIGURE 1 | Frequency response under GSCs with different magnitudes. (a) A strong GSC can immediately alter the power imbalance from generation shortage to generation surplus. (b) A weak GSC can reduce the generation shortage.

shows a strong GSC that can immediately alter the power imbalance. In this case, the critical switching time will be equal to the time when the trajectory reaches the safety limit. If the GSC is not strong enough to alter the power imbalance, the frequency will continue declining at a lower rate. In this case, we should switch to the supportive control mode before reaching the safety limit (Figure 1b). This critical switching time will be estimated in this study. In addition, both GSC-induced impact scenarios shown in Figure 1 should be taken into account [8, 38]. The proposed control structure is capable of handling both scenarios.

The diesel-wind energy system is one of the most widely deployed power resources subject to the aforementioned challenges. Without loss of generality, we employ a diesel-wind energy system as the physical plant for control design. Nevertheless, the proposed methodology can be applied to any microgrid powered by renewable energy resources and synchronous generators.

3.1 | Diesel-Wind System Modeling

This section illustrates the mathematical model of the dieselwind plant for controller design. Unlike the simulation models in Section 5 where every component is modeled, this section focuses on the components related to frequency control. As pointed out by many researchers, deriving a reduced-order model for a wind turbine generator (WTG) that represents the full-order model features is a challenging task. The selective modal analysis (SMA)-based model reduction has been adopted in this study to obtain the reduced order model of the augmented plant, and it will be shown that it is successful in capturing the active power variation of a WTG. A detailed derivation of the SMA model reduction is provided in [39]. We will adopt the SMA-based reduced-order model of the WTG derived in [40] to design our control and verify it with the nonlinear model in simulations. However, for the sake of consistency, the derivation is briefly stated in this subsection.

The dynamics of the DFIG-based wind turbine (defined later) are represented by a reduced-order model based on the SMA model reduction method [39]. In this method, the most relevant dynamic of the WTG to the active power output is the rotor speed $(\Delta\omega_r)$, which has the highest participation to capture the relevant active power dynamics of the WTG. Therefore, the reduced-order model of the WTG can be expressed by this state variable, considered as the most relevant state, and the reduced model of the DFIG based wind turbine can be represented as the following 1st-order model.

$$\Delta \dot{\omega}_r = A_{rd} \Delta \omega_r + B_{rd} u$$

$$\Delta P_g = C_{rd} \Delta \omega_r + D_{rd} u$$
(8)

where u is the supplementary input of the GSC, and ΔP_g is the active power variation of the WTG due to the inertia emulation signal u. The corresponding matrices A_{rd} , B_{rd} , C_{rd} , and D_{rd} are given in Appendix A together with the full-order differential-algebraic model of the WTG and a detailed presentation of the SMA model reduction (see [40] and [39] for more details).

A diesel synchronous generator (DSG) is a combustion engine driven synchronous generator. A complete model consists of

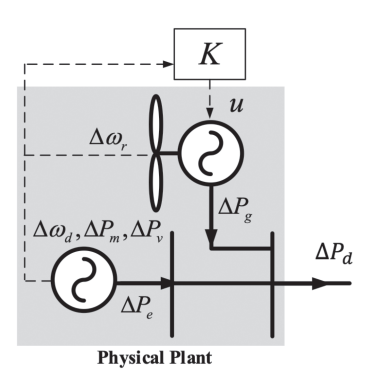


FIGURE 2 | Feedback control of a diesel-wind energy system for frequency.

the synchronous generator, combustion engine, governor, and exciter. The frequency dynamics of this system can be represented by the classic SFR model as a simplification of the original full-order model by (see [40])

$$2H\Delta\dot{\omega} = f\left(\Delta P_m - (\underline{\Delta P_d - \Delta P_g})\right)$$

$$\tau_d\Delta\dot{P}_m = -\Delta P_m + \Delta P_v$$

$$\tau_s\Delta\dot{P}_v = -\Delta P_v - \frac{\Delta\omega}{fR_D}$$
(9)

where H is the inertia constant, $\Delta\omega$ is the frequency variation, ΔP_m is the mechanical power deviation, ΔP_d is the measured power flow variation at the location illustrated in Figure 2 that is regarded as the disturbance, ΔP_g is the active power variation for the doubly fed induction generator (DFIG)-based wind turbine, and $\Delta P_e = \Delta P_d - \Delta P_g$ is the electrical power deviation. ΔP_v is the valve position deviation, R_D is the governor droop setting, f is the speed base of the generator, τ_d and τ_s are the engine and governor time constants respectively.

The state space representation of the reduced-order model, which is used as an aggregated model of the DFIG-based WTG represented by (8)) and the DSG represented by (9) with the state feedback control strategy illustrated in Figure 2, is defined by

$$\dot{x} = Ax(t) + B_2 u + B_1 d(t); \quad y = Cx(t)$$
 (10)

where the state $x = [\Delta \omega, \Delta P_m, \Delta P_v, \Delta \omega_r]^T$, the feedback control input u = Kx (K is the matrix to be designed), the disturbance $d(t) = \Delta P_d$, and y is the output measurement. The system (10) is described by the following matrices

$$A = \begin{bmatrix} 0 & \frac{f}{2H} & 0 & \frac{fC_{rd}}{2H} \\ 0 & \frac{-1}{\tau} & \frac{1}{\tau} & 0 \\ \frac{-1}{f\tau_s R_D} & 0 & \frac{-1}{\tau_s} & 0 \\ 0 & 0 & 0 & A_{rd} \end{bmatrix}, B_2 = \begin{bmatrix} \frac{fD_{rd}}{2H} \\ 0 \\ 0 \\ B_{rd} \end{bmatrix}$$

$$B_1 = \begin{bmatrix} \frac{-f}{2H} & 0 & 0 & 0 \end{bmatrix}^T, \ C = \begin{bmatrix} 1 & 0 & 0 & 0 \end{bmatrix}$$

3.2 | Switching Synthesis and Control Design for Safety Region

A power system, modeled in (10), is considered to go through changes in configuration in three modes as a switched system. The first mode is the pre-fault mode when the system is operating at a steady-state x_{ss} . For this mode, it is considered that the system is operating at a known steady-state equilibrium point, say without loss of generality, $x_{ss} = 0$). Suppose that at time t_s a disturbance occurs that changes the structure of the system, but the support of the DFIG-based wind turbine is not activated and is described by the second mode which is the fault-on mode. The third one is the controlled mode, where the supportive control is activated. The power system becomes then a switched system described by the following two differential equations:

$$\dot{x} = \begin{cases} Ax + B_1 d(t), & \text{for } t_s \le t \le t_1 \\ Ax + B_1 d(t) + B_2 u, & \text{for } t_1 < t < \infty \end{cases}$$
 (11)

 $x(t) \in \mathbb{R}^n$ is the vector state, A, B_1, B_2 are constant matrices with appropriate dimensions, u is the control input, and $d(t) \in \mathcal{D}$ is the disturbance. The first subsystem is the fault-on mode and the second one is the controlled mode, where the supportive control is activated at t_1 to limit the deviation of trajectories following the perturbation. When the fault occurs, the trajectory of the system will be driven away from x_{ss} . At t_1 , the supportive control will be activated and the system is henceforth governed by the second dynamics in (11). Note that, $x(t_1)$ will be the initial state of the controlled mode, and whether or not the system will stay in a safety region depends on whether $x(t_1)$ belongs to some region determined according to the post-fault system equation. A crucial factor in determining how far $x(t_1)$ could be from x_{ss} is the time needed to remove the fault, that is, the time difference $(t_1 - t_s)$. If $(t_1 - t_s)$ is very short, then, by the continuity of the solution for t, it is very likely that the trajectory does not reach the unsafe set. However, one needs time to detect the fault and clear it as shown in Figure 1. In planning such a system, it is valuable to estimate the critical time, say t_c , such that the controller has to be activated within this time, that is, $t_1 - t_s \le t_c$ to prevent the trajectory to reach the unsafe region. This concept is similar to the critical clearing time in transient stability analysis. This work aims to design such a controller and estimate the critical time.

Let the safe set X_S , where the frequency response is adequate, that is, $\omega \in X_S = \{x \in X : \omega_{lim}^- \le \omega \le \omega_{lim}^+ \}$, and its complementary, $X_U = \{x \in X : \omega > \omega_{lim}^+ \text{ or } \omega < \omega_{lim}^- \}$, which is the unsafe set. Let \mathcal{X}_S , the set characterized by a safety metric, $\mu(x,y) = \sqrt{(x-y)^T P(x-y)}$, $P = P^T > 0$, be

$$\mathcal{X}_s = \{ x \in \mathcal{X} : \mu(x, 0) \le d_u \} \tag{12}$$

for some constant $d_u > 0$, where \mathcal{X} is the state space of the perturbed system in (11). For simplicity, $\mu(x,0)$ is abbreviated by $\mu(x)$. Note that, the initial states \mathcal{X}_0 of the controlled system in (11) may be any subset of \mathcal{X}_s . Let the barrier function $B(x) = \mu^2(x) - d_u^2 = x^T P x - d_u^2$, and the corresponding set be

$$S(P, d_n^2) = \{x \in \mathcal{X} : x^T P x \le d_n^2\} = \{x \in \mathcal{X} : B(x) \le 0\}$$
 (13)

The objective is that, when a fault occurs, we have to activate the WTG supportive mode, at t_1 , when the trajectory

reaches the boundary of $S(P, d_u^2)$, so that $x(t_1) \in \partial S(P, d_u^2) = \{x \in \mathcal{X} : x^T P x = d_u^2\}$ to achieve adequate frequency response (i.e., bounded within the defined safe set X_S). $\partial S(P, d_u^2)$ denotes the boundary of the set $S(P, d_u^2)$.

4 | Main Results

Consider the closed loop switched system (11) with the control feedback u = Kx,

$$\dot{x} = \begin{cases} Ax + B_1 d(t), & \text{for } t_s \le t \le t_1 \\ (A + B_2 K)x + B_1 d(t), & \text{for } t_1 < t < \infty \end{cases}$$
 (14)

where $t_s = 0$, without loss of generality, and $d(t) \in \mathcal{D}$ is a finite-energy disturbance metric such that

$$\int_0^t \|d(s)\|^2 ds \le \alpha < \infty \tag{15}$$

Suppose that the safety region of the controlled subsystem is given by the set:

$$S(P,\rho) = \{ x \in X : x^T P x \le \rho \}$$
 (16)

where $P=P^T>0$ is a given positive definite matrix and ρ is a known positive number. The boundary of this set, denoted by $\partial S(P,\rho)=\{x\in X: x^TPx=\rho\}$, is the ellipsoid that separates the safe set X_S and the unsafe set X_U . We will design a feedback control law u(x)=Kx, such that the trajectories of the system (14) remain in the safety region $S(P,\rho)$ and never reach the unsafe set.

Note that the original safety region of a power system is described by boxes since most states should vary between certain lower and upper bounds. However, box-type constraints are computationally complicated. Hence, we use ellipsoids that are described by the matrix P to approximate the box constraints as close as possible. The computation of P can be performed using the so-called maximum volume inscribed ellipsoid algorithms that have been well studied [41]. The benefit is that ellipsoids can be easily incorporated into convex optimization for the control design.

4.1 | Control Design

Theorem 2. Consider the switched system (14) with the perturbation satisfying (15). Let the safety region determined by (16) and the corresponding positive definite function $V(x(t)) = x^T(t)Px(t)$, with $P = P^T > 0$ given. Suppose that for $t = t_1$, $V(x(t_1)) \le \rho - \varepsilon$, for $\rho > \varepsilon > 0$. If there exists a matrix K and a positive constant $\eta \le \frac{\varepsilon}{\alpha}$ such that

$$((PB_2)K)^T + (PB_2)K + \left[A^TP + PA + \frac{1}{\eta}PB_1B_1^TP\right] \le 0 \qquad (17)$$

then the solution of (14) always remains inside the safety region $S(P,\rho)$. On the other hand, the matrix K satisfying (17) exists if and only if

$$(PB_2)^{\perp} \left[A^T P + PA + \frac{1}{\eta} P B_1 B_1^T P \right] ((PB_2)^{\perp})^* < 0$$
 (18)

or

$$(PB_2)(PB_2)^* > 0 (19)$$

Further assume that $(PB_2)^*(PB_2) > 0$. Then all matrices K are given by

$$K = -\gamma (PB_2)^* + \sqrt{\gamma} L\Omega^{\frac{1}{2}}$$
 (20)

where L is any matrix such that $||L|| \le 1$ and γ is a positive scalar such that

$$\Omega = \gamma (PB_2)(PB_2)^* - \left(A^TP + PA + \frac{1}{\eta}PB_1B_1^TP\right) > 0$$
 (21)

Proof. Let the positive definite function $V(x) = x^T P x$. The derivative of V along the second subsystem's trajectory in (14) is given by

$$\dot{V}(x) = x^{T}[(A + B_{2}K)^{T}P + P(A + B_{2}K)]x + 2x^{T}PB_{1}d(t)$$
 (22)

Note that, the following inequality is always satisfied

$$2x^TPB_1d(t) \leq \frac{1}{\eta}x^TPB_1B_1^TPx + \eta d(t)^Td(t), \quad \forall \eta > 0$$

So, we can derive from (22) the following

$$\dot{V}(x) \le x^{T} [(A + B_{2}K)^{T}P + P(A + B_{2}K)]x$$

$$+ \frac{1}{\eta} x^{T} P B_{1} B_{1}^{T} P x + \eta d(t)^{T} d(t)$$

$$= x^{T} [(A + B_{2}K)^{T} P + P(A + B_{2}K)$$

$$+ \frac{1}{\eta} P B_{1} B_{1}^{T} P x + \eta d(t)^{T} d(t)$$
(23)

Suppose that there exists a matrix K satisfying condition (17), we get

$$(A + B_2 K)^T P + P(A + B_2 K) + \frac{1}{\eta} P B_1 B_1^T P \le 0$$

which implies that

$$\dot{V}(x(t)) \le \eta d(t)^T d(t)$$

By integrating both sides of this inequality for $t_1 \le t < \infty$, and by considering condition (15), we have

$$V(x(t)) \le V(x(t_1)) + \eta \int_{t_1}^t d^T(\tau) d(\tau) d\tau$$

$$\le V(x(t_1)) + \eta \alpha, \quad \forall t \ge t_c$$

Since at $t=t_1$, $x(t_1)$ is inside the set $S(P,\rho-\varepsilon)$, such that $V(x(t_1)) \leq \rho-\varepsilon$, we obtain

$$V(x(t)) \le \rho - \varepsilon + \eta \alpha, \quad \forall t \ge t_1$$

(i.e., $x^T(t)Px(t) \le \rho - \varepsilon + \eta \alpha$, $\forall t \ge t_1$) which implies that

$$x(t) \in S(P, \rho - \varepsilon + \eta \alpha), \quad \forall t \ge t_1$$

We conclude that for $0 \le \eta \le \frac{\varepsilon}{\alpha}$, we have $V(x(t)) \le \rho - \varepsilon + \eta \alpha < \rho$, $\forall t \ge t_1$, which implies that $x(t) \in S(P, \rho - \varepsilon + \eta \alpha) \subset S(P, \rho - \varepsilon + \eta \alpha)$

 $S(P, \rho)$, $\forall t \ge t_1$. This means that the trajectories of the closed-loop subsystem starting from x(t), $\forall t_s \le t \le t_1$ (i.e., from the set $S(P, \rho - \varepsilon)$) will remain inside $S(P, \rho)$ for all $t > t_1$, and for each finite energy disturbance d(t) satisfying (15), which ensures the safety of the system.

On the existence of the matrix K:

Let $F = (PB_2)$ and $Q = (A^TP + PA + \frac{1}{\eta}PB_1B_1^TP)$. The inequality (17) is equivalent to

$$(FK) + (FK)^T + Q \le 0$$

From Theorem 1, the matrix *K* exists if and only if

$$(F)^{\perp}Q(F^{\perp})^T < 0 \quad \text{or} \quad FF^T > 0$$

Further, assuming that $F^TF > 0$, then K is given by

$$K = -\gamma F^T + \sqrt{\gamma} L \Omega^{\frac{1}{2}} \tag{24}$$

where L is any matrix, with $\|L\| \le 1$, and γ is a positive scalar such that

$$\Omega = \gamma F F^T - Q > 0 \tag{25}$$

which concludes the proof.

The existence of γ in (25) is ensured by Finsler's Lemma [42, 43]. Its computation is presented in Appendix B.

Remark 1. If (PB_2) is a full rank matrix, then the matrix K exists if and only if condition (19) is satisfied.

Remark 2. The previous result is directly related to the barrier function B(x). Specifically, it has been shown that the derivative of $V = x^T P x$ along the trajectories of the controlled system in (14) satisfies (23), which implies that, and according to (17),

$$\dot{V}(x) - \eta d^{T}(t)d(t) \le x^{T} \left[(A + B_{2}K)^{T}P + P(A + B_{2}K) + \frac{1}{\eta}PB_{1}B_{1}^{T}P \right] x < 0$$
(26)

We have

$$\dot{V}(x) - \eta d^{T}(t)d(t) = \frac{d}{dt} \left[V(x) - \eta \int_{t_s}^{t} d^{T}(s)d(s) \ ds \right]$$
 (27)

Let the barrier function B(x, d), which depends on the perturbation, be defined as

$$B(x,d) = \left[V(x) - \eta \int_{t_s}^t d^T(s)d(s) \ ds \right] - \rho + \varepsilon$$

$$\geq x^T P x - \eta \alpha - \rho + \varepsilon$$
(28)

Let the initial set of the controlled system in (14) be

$$\mathcal{X}_0 = \{ x \in \mathcal{X} : x^T P x \le \rho - \varepsilon \}$$
 (29)

and the unsafe region

$$\mathcal{X}_{n} = \{ x \in X : x^{T} P x \ge \rho \} \tag{30}$$

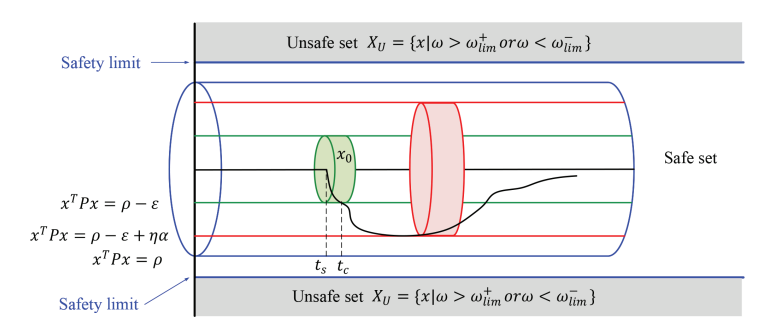


FIGURE 3 | Safety limit, safety region, safe and unsafe sets: The controller is applied when the trajectory reaches the boundary $x^T P x = \rho - \varepsilon$ (or before) such that the trajectory of the controlled system will remain in the set $\{x : x^T P x \le \rho - \varepsilon + \eta \alpha\}$.

The barrier function B(x, d) satisfies the safety conditions described in Lemma 1, such that

- 1. $B(x,d) \le 0 \Rightarrow x^T P x \le \rho \varepsilon + \eta \alpha, \quad \forall x \in \mathcal{X}_0$
- 2. $B(x,d) > 0 \Rightarrow x^T Px > \rho \varepsilon + \eta \alpha, \quad \forall x \in \mathcal{X}_u$
- 3. $\frac{\partial B(x,d)}{\partial x}[(A+B_2K)x+B_1d(t)]<0, \ \forall (x,d)\in (\mathcal{X}\times\mathcal{D})$ according to (26) and (27).

Then the safety is guaranteed and B(x, d) = 0 represents a barrier certificate of the system (see Figure 3).

Remark 3. Note that the control matrix K depends on ε and the energy of the perturbation α , since it depends on η . If we choose $\eta\alpha\approx\varepsilon$ (i.e., $-\varepsilon+\eta\alpha\approx0$), the set $\partial S(P,\rho-\varepsilon+\eta\alpha)$ will be close to $\partial S(P,\rho)$, and the designed controller will reflect the case in Figure 1a. If we choose $\eta\alpha>\varepsilon$, the designed controller will reflect the case in Figure 1b.

4.2 | Estimation of the Critical Time

In this section, we give an estimation of the critical time $t_c = t_1 - t_s$ based on the perturbation. This critical time is described as the time that the trajectories of the perturbed system take to reach the boundary of \mathcal{X}_0 so that

$$x(t_1)^T P x(t_1) = \rho - \varepsilon \tag{31}$$

The solution $x(t_1)$ can be derived from the perturbed system (14) as follows:

$$x(t_1) = e^{A(t_1 - t_s)} x(t_s) + \int_{t_s}^{t_1} e^{A(t_1 - \tau)} B_1 d(\tau) d\tau$$

with $x(t_s) = 0$. According to Lemma 2, we have

$$x(t_{1})^{T}Px(t_{1})$$

$$= \left[\int_{t_{s}}^{t_{1}} e^{A(t_{1}-\tau)} B_{1}d(\tau) d\tau \right]^{T} P \left[\int_{t_{s}}^{t_{1}} e^{A(t_{1}-\tau)} B_{1}d(\tau) d\tau \right]$$

$$\leq (t_{1}-t_{s}) \int_{t_{s}}^{t_{1}} (e^{A(t_{1}-\tau)} B_{1}d(\tau))^{T} P (e^{A(t_{1}-\tau)} B_{1}d(\tau)) d\tau$$

$$\leq t_{c} ||B_{1}||^{2} \alpha \lambda_{\max} (e^{A^{T}t_{c}} P e^{At_{c}})$$
(32)

The above inequality is obtained using integration by parts. Finally, we get the estimation of the critical time t_c as

$$t_c ||B_1||^2 \alpha \lambda_{\max}(e^{A^T t_c} P e^{A t_c}) = \rho - \varepsilon$$
 (33)

which can be easily computed. In particular, if d(t) is a constant step perturbation, we have

$$x(t_1) = \int_{t_s}^{t_1} e^{A(t_1 - \tau)} B_1 d(\tau) d\tau = \left[e^{A(t_1 - t_s)} - I \right] A^{-1} B_1 d(t_1)$$
 (34)

The critical time, in this case, can be estimated as follows:

$$x(t_{1})^{T}Px(t_{1}) = d^{T}(t_{1})B_{1}^{T}(e^{A^{T}(t_{1}-t_{s})} - I)A^{-T}PA^{-1}$$

$$\times (e^{A(t_{1}-t_{s})} - I)B_{1}d(t_{1})$$

$$\leq \lambda_{\max}(A^{-T}PA^{-1})d^{T}(t_{1})B_{1}^{T}(e^{A^{T}t_{c}} - I)$$

$$\times (e^{At_{c}} - I)B_{1}d(t_{1})$$
(35)

and t_c can be estimated by

$$\lambda_{\max}(A^{-T}PA^{-1})B_1^T(e^{A^Tt_c} - I)(e^{At_c} - I)B_1 = \frac{\rho - \varepsilon}{d^2(t)}$$
 (36)

Remark 4. Intuitively, and according to the critical time estimation given in (33) and Figure 3, we can remark that if we fix the bounds ρ and $\rho - \varepsilon$ and increase the perturbation, the trajectory will reach faster the boundary of the ellipsoid $S = \{x : x^T P x = \rho - \varepsilon\}$, which means that we will need a shorter critical time. Inversely, if we make $\rho - \varepsilon$ larger, the trajectory takes more time to reach the boundary of the ellipsoid $S = \{x : x^T P x = \rho - \varepsilon\}$, which means that the critical time here can be longer. To see this, we can use an equivalent state-space representation for the triplet (A, B_1, C) , proposed in [44]. The idea is, if h(t) is the impulse response corresponding to (A, B_1, C) (i.e., $h(t) = Ce^{At}B_1$), there exist continuous matrix functions $\tilde{B}(t)$ and $\tilde{C}(t)$ such that:

$$h(t) = Ce^{At}B_1 = \tilde{C}(t)\tilde{B}(t)$$
(37)

The corresponding equivalent state space realization is then:

$$\dot{\tilde{x}} = \tilde{B}(t)d(t), \quad y(t) = \tilde{C}(t)\tilde{x}(t) \tag{38}$$

The merit of this realization is that the state matrix is the zero matrix, but it is time varying albeit representing the same LTI system. The matrices $\tilde{B}(t)$ and $\tilde{C}(t)$ are given by the singular values and the Schmidt pairs of the Hankel operator corresponding

to (A, B_1, C) (see [44] for the details.) Now, since $\tilde{B}(t)$ is continuous, $\|\tilde{B}(t)\|$ is uniformly bounded over the interval $[t_s, t_1]$, so $\max_{t_s \leq t \leq t_1} \|\tilde{B}(t)\| = b < \infty$, for some finite positive constant b. An analogous reasoning to get (33) yields an estimate of the critical time as follows:

$$\rho > t_c b^2 \alpha \lambda_{\max}(P) = \rho - \varepsilon \Rightarrow \frac{\rho}{b^2 \alpha} > t_c = \frac{\rho - \varepsilon}{b^2 \alpha \lambda_{\max}(P)}$$

This expression shows clearly how the critical time varies as a function of ρ , ε and the size of the perturbation α . If the bounds ρ or $\rho - \varepsilon$ increase and α is fixed, the critical time t_c increases, as more time is allowed to reach the boundary of S, while if the perturbation' size α is increased while ρ and $\rho - \varepsilon$ are fixed, the critical time t_c decreases.

5 | Numerical Results

The suggested control structure is applied to the modified 33-bus microgrid system in MATLAB Simulink platform. The closed-loop system performance is tested using the diesel-wind system described in [40, 45]. The wind turbine generator model is modified based on the DFIG in the Simulink demo library by changing the aerodynamic model to the one detailed in [39], where a two-mass model is reduced to the swing equations with combined inertia of the turbine and generator.

5.1 | Model Reduction Validation

As described before, the analytical model for the control design consists of the reduced-order model of the WTG in (8) and the 3rd-order frequency response model of the diesel generator in (9). This subsection illustrates the comparative simulations between the full-order and the reduced-order model of the WTG. Figure 4 illustrates the frequency responses between the swing-turbine-governor model and a full-order synchronous generator. Their differences are negligible. The responses of the nonlinear system, full linear, and reduced order linear models of the WTG are compared in Figure 5 in order to validate the SMA model reduction technique. As observed, the SMA successfully captures the active power related dynamics of the full linear system, and the induced error by the SMA-based model reduction is not significant. Hence, the control design procedure can be performed based on the reduced order model with enough accuracy compared to the detailed nonlinear model as shown in Figure 5.

5.2 | Closed-Loop Verification of the Linearized System

The overall reduced order model defined in (10) is considered for the design control procedure with the following parameters:

$$H = 1s$$
, $\tau_s = 0.1s$, $\tau = 0.2s$, $f = 60Hz$, $A_{rd} = -0.27$

$$B_{rd} = 0.2624, C_{rd} = 0.56, D_{rd} = -0.5355, R_D = 0.05$$

where we have

$$A = \begin{bmatrix} 0 & 30 & 0 & 16.79 \\ 0 & -5 & 5 & 0 \\ -3.333 & 0 & -10 & 0 \\ 0 & 0 & 0 & -0.27 \end{bmatrix}, B_2 = \begin{bmatrix} -16.06 \\ 0 \\ 0 \\ 0.262 \end{bmatrix}, B_1 = \begin{bmatrix} -30 \\ 0 \\ 0 \\ 0 \end{bmatrix}, \text{ and }$$

$$C = \begin{bmatrix} 1 & 0 & 0 & 0 \end{bmatrix}$$

Here, the disturbance is assumed to be a d(t) = 0.1MW = 0.1 (p.u) load change at Bus 18 that occurs at t = 3 s and clears at t = 8 s, with energy $\alpha = \int_{3s}^{8s} d^2(s) ds = 0.05$. he first objective is to design a feedback controller to ensure the safety of the frequency performance. Let the barrier function B(x, d), the sets \mathcal{X}_0 and \mathcal{X}_u be as in (28), (29), and (30), respectively, with $\rho = 1, \varepsilon = 0.8$,

$$\eta = 10 < \frac{\varepsilon}{\alpha} = 16, \text{ and } P = \begin{bmatrix} 4 & 0 & 0 & 0\\ 0 & 1.2346 & 0 & 0\\ 0 & 0 & 0.444 & 0\\ 0 & 0 & 0 & 1 \end{bmatrix}$$

The barrier function is computed based on the safe operating area [40] such that $|\Delta\omega|<0.5$. For that, the matrix P is computed to get the largest ellipsoid inscribed in the safety limit bounds (see [41, 46]). Its zero level set is given by the ellipsoid $\partial S = \{x \in \mathbb{R}^4 : x^T P x = \rho - \varepsilon + \eta \alpha\}$ as shown in Figure 6. The control matrix is

$$K = -\gamma (PB_2)^* + \sqrt{\gamma} L\Omega^{\frac{1}{2}} = [0.32 \quad 0 \quad 0 \quad -0.0013]$$

with $\Omega = \gamma (PB_2)(PB_2)^T - (A^TP + PA + \frac{1}{\eta}PB_1B_1^TP)$, $\gamma = 0.005$, and $L = [0.5 \ 0 \ 0]$. The controller K satisfies the safety condition (17) in Theorem 2 so that

$$((PB_2)K)^T + (PB_2)K + \left[A^TP + PA + \frac{1}{\eta}PB_1B_1^TP\right] \le 0$$

The frequency responses of the linearized model with and without control at different critical times are shown in Figure 7. Using

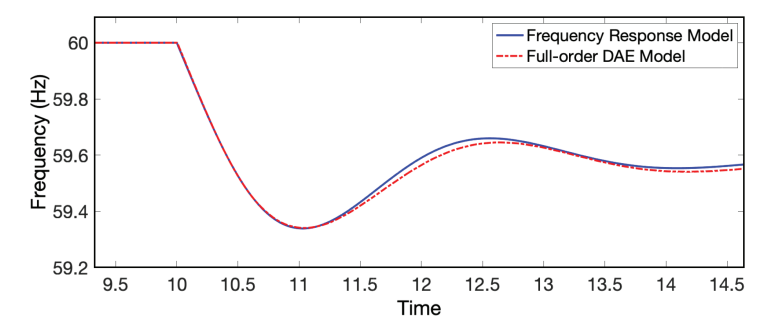


FIGURE 4 | Frequency responses of the swing-turbine-governor model and the full-order synchronous generator.

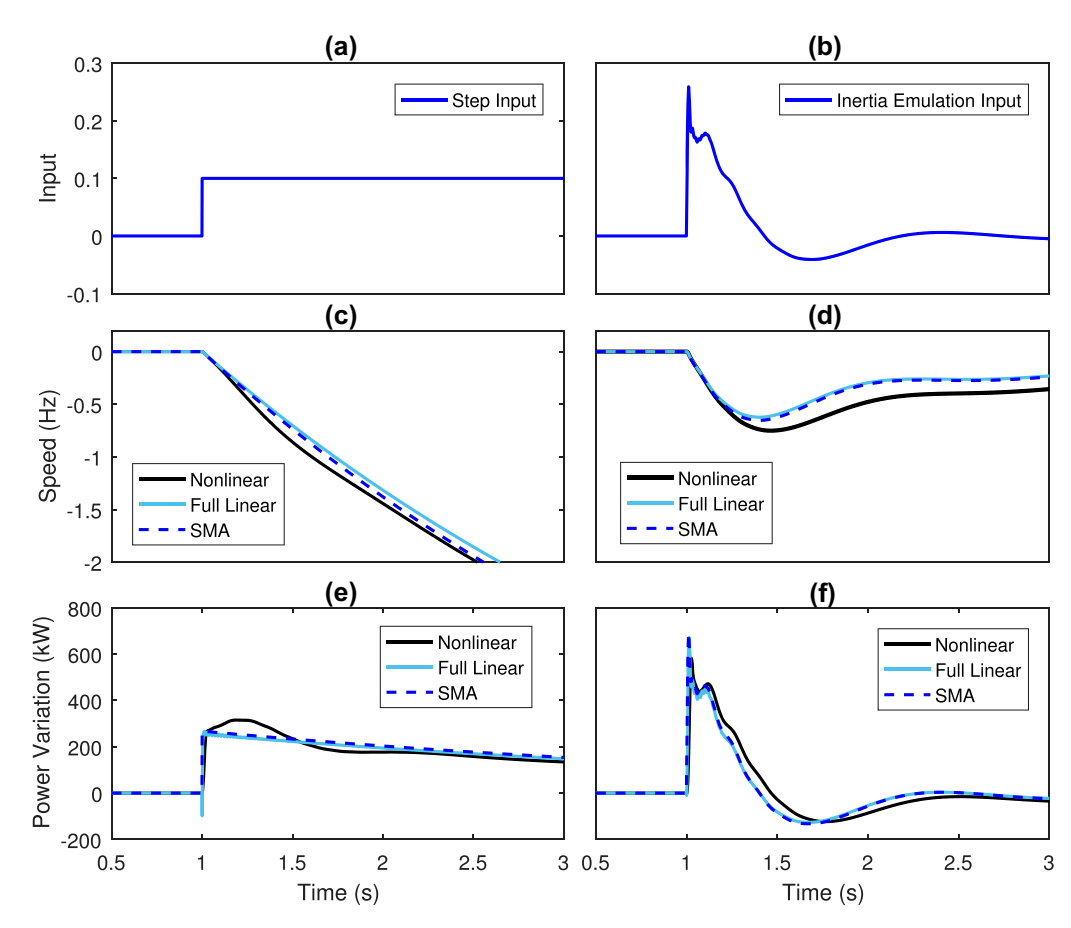


FIGURE 5 | Response comparison of nonlinear, linear and SMA-based first-order WTG model under step input and inertia emulation input. (a) Step input. (b) Inertia emulation input via washout filter. (c) WTG speed variation under step input. (d) WTG speed variation under inertia emulation input. (e) WTG active power variation under step input. (f) WTG active power variation under inertia emulation input.

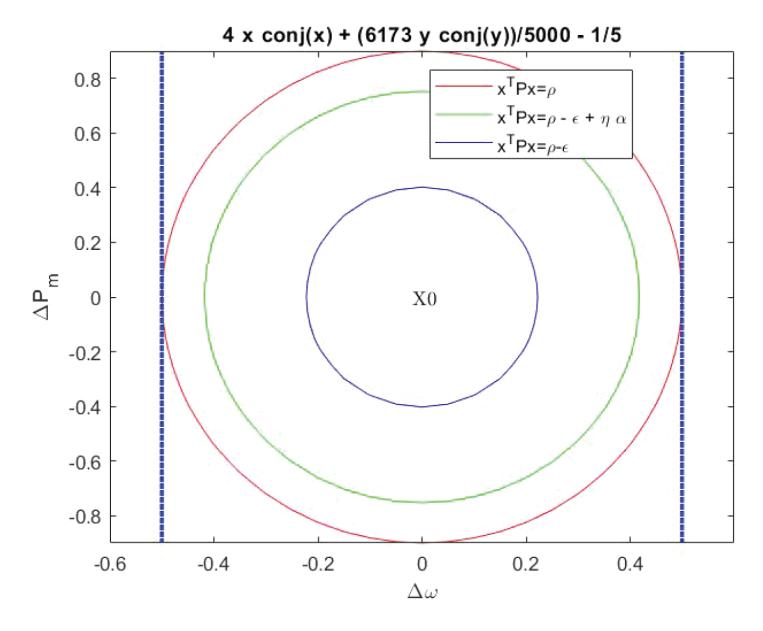


FIGURE 6 | Level sets of the barrier function B(x, d).

simulation, we can see that if the controller is applied later than $t_c=3.179$, the frequency reaches the unsafe set. By computing the critical time analytically according to (36), we get $t_c=3.09$ which approximates well the critical time and guarantees the safety of the frequency response.

5.3 | Closed-Loop Verification of the Nonlinear System

The frequency response of the nonlinear system using the controller K is shown in Figure 8. The obtained controller is applied

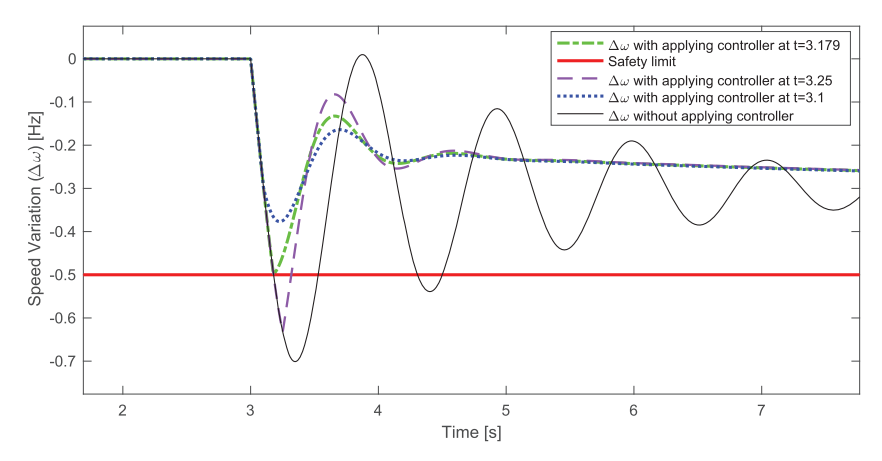


FIGURE 7 | Closed-loop linearized model response, DSG speed.

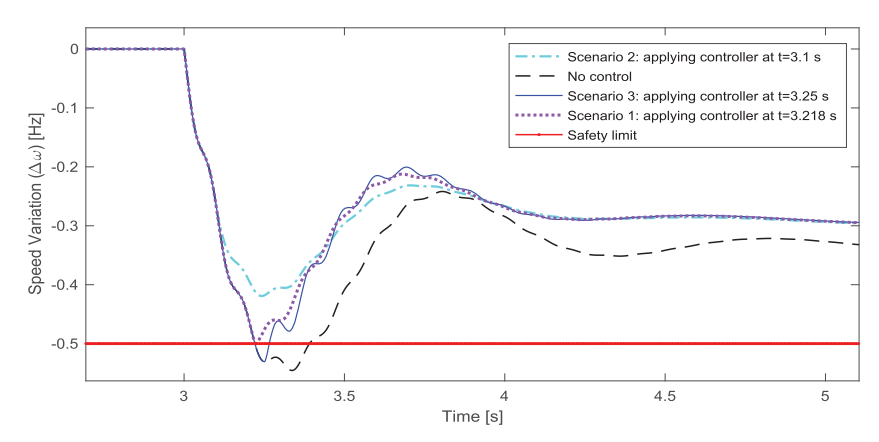


FIGURE 8 | DSG speed under feedback control applied at different times with 0.1 (p.u) load change as a disturbances at bus 18.

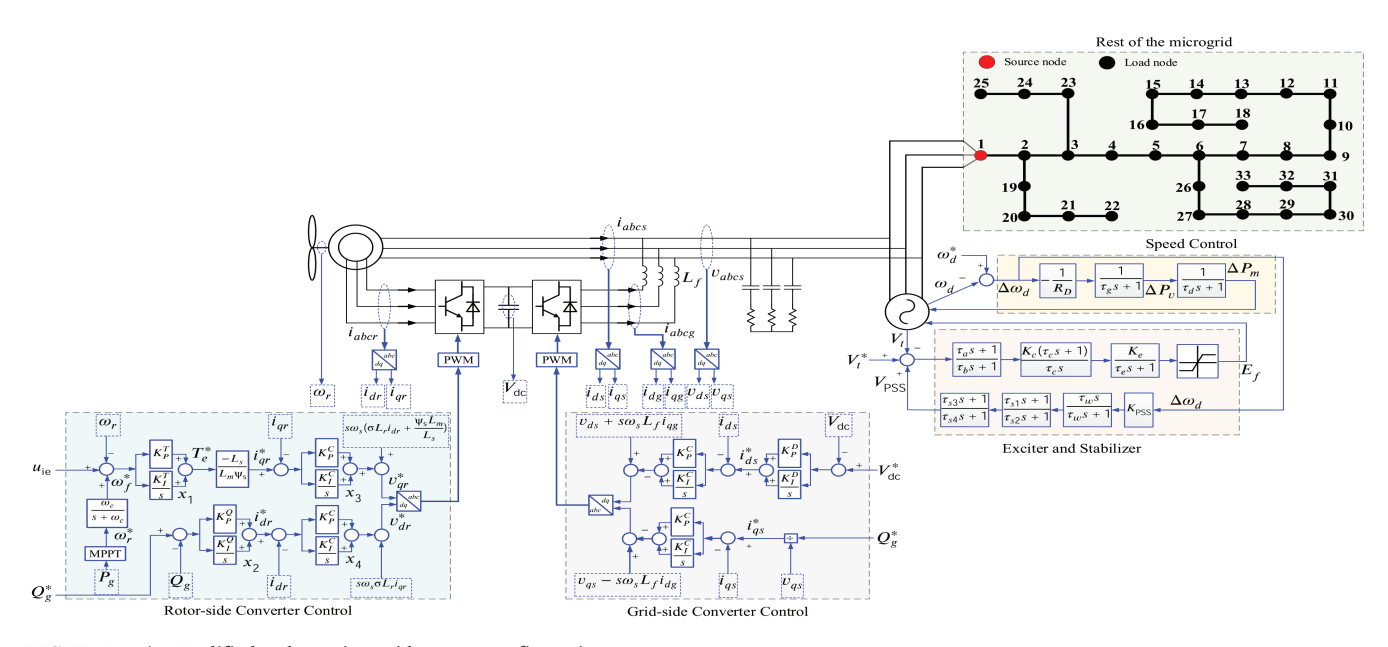


FIGURE 9 | Modified 33 bus microgrid system configuration.

on the nonlinear full-order model with all detail shown in Figure 9 [45]. We can see that this controller prevents the frequency from reaching the unsafe set if it is applied before $t_c = 3.218$ as the critical time. Three scenarios are considered in the

closed-loop system performance by applying the controller at different times to show the effectiveness of the proposed approach, including the computation of critical time with performance guarantees.

- *Scenario 1*: The controller is applied at t = 3.218 s which is the critical time obtained from the proposed method. Clearly, the speed deviation will be tangent to the unsafe range but it will not cross it.
- *Scenario 2*: The controller is applied to the system at $t=3.1\,\mathrm{s}$ which is less than the computed critical time. In this case, the performance is still guaranteed since it will not cross the unsafe range defined for the speed deviation.
- *Scenario 3*: The controller is applied after the critical time at t=3.25 s. As seen, the controller can still react to reduce the speed deviation, but it will pass the safety limit. We can see that the critical time computed analytically $t_c=3.09$ estimates reasonably the time needed to apply the controller in order to prevent the frequency to reach the unsafe limit for the nonlinear system too.

6 | Conclusion

This article deals with a novel safety feedback control design for islanded microgrids, where the system considered switches between the normal mode to a faulted mode when a disturbance occurs, and to a post-fault mode when a supportive controller is applied. The power system model considered is a DSG connected to a WTG. The supportive control feedback law from the WTG is designed to guarantee the safety of the frequency response and avoid reaching the unsafe region. The critical time has been estimated analytically and compared to nonlinear full-order model simulation. The obtained results show the effectiveness of the proposed approach for guaranteed adequate frequency performance.

Conflicts of Interest

The authors declare no conflicts of interest.

Data Availability Statement

Data sharing not applicable as no new data generated, or the article describes entirely theoretical research.

Endnotes

1 The term *safety* is adopted from the control literature and in this context means a well-defined and allowable operating region. A safe response means the trajectories of all concerned states stay within the defined safe limits. In this article, safety and adequacy of a frequency trajectory refer to the same definition and will be used interchangeably.

References

- 1. A. Ulbig, T. S. Borsche, and G. Andersson, "Impact of Low Rotational Inertia on Power System Stability and Operation," in *Proceedings of the 19th IFAC World Congr* 47, no. 3 (2014), 7290–7297.
- 2. Q. Hong, M. Karimi, M. Sun, et al., "Design and Validation of a Wide Area Monitoring and Control System for Fast Frequency Response," *IEEE Transactions on Smart Grid* 11, no. 4 (2020): 3394–3404, https://doi.org/10.1109/TSG.2019.2963796.
- 3. S. Pulendran and J. E. Tate, "Energy Storage System Control for Prevention of Transient Under-Frequency Load Shedding," *IEEE Transactions on Smart Grid* 8, no. 2 (2017): 927–936.

- 4. D. Zhao, C. Zhang, Y. Sun, S. Li, B. Sun, and Y. Li, "Distributed Robust Frequency Restoration and Active Power Sharing for Autonomous Microgrids With Event-Triggered Strategy," *IEEE Transactions on Smart Grid* 12, no. 5 (2021): 3819–3834, https://doi.org/10.1109/TSG.2021.3087960.
- 5. R. É. G. de Almeida and J. A. Pecas Lopes, "Participation of Doubly Fed Induction Wind Generators in System Frequency Regulation," *IEEE Transactions on Power Systems, IEEE Transactions on Power Systems* 22, no. 3 (2007): 944–950, https://doi.org/10.1109/TPWRS.2007.901096.
- 6. D. Gautam, L. Goel, R. Ayyanar, V. Vittal, and T. Harbour, "Control Strategy to Mitigate the Impact of Reduced Inertia Due to Doubly Fed Induction Generators on Large Power Systems," *IEEE Transactions on Power Systems* 26, no. 1 (2011): 214–224, https://doi.org/10.1109/TPWRS .2010.2051690.
- 7. M. F. M. Arani and E. F. El-Saadany, "Implementing Virtual Inertia in DFIG-Based Wind Power Generation," *IEEE Transactions on Power Systems* 28, no. 2 (2013): 1373–1384, https://doi.org/10.1109/TPWRS.2012.2207972.
- 8. Y. Zhang, M. E. Raoufat, K. Tomsovic, and S. M. Djouadi, "Set Theory-Based Safety Supervisory Control for Wind Turbines to Ensure Adequate Frequency Response," *IEEE Transactions on Power Systems* 34, no. 1 (2019): 680–692.
- 9. G. Lalor, A. Mullane, and M. O'Malley, "Frequency Control and Wind Turbine Technologies," *IEEE Transactions on Power Systems* 20, no. 4 (2005): 1905–1913, https://doi.org/10.1109/TPWRS.2005.857393.
- 10. M. Kayikci and J. V. Milanovic, "Dynamic Contribution of DFIG-Based Wind Plants to System Frequency Disturbances," *IEEE Transactions on Power Systems* 24, no. 2 (2009): 859–867, https://doi.org/10.1109/TPWRS.2009.2016062.
- 11. L. Wu and D. G. Infield, "Towards an Assessment of Power System Frequency Support From Wind Plant—Modeling Aggregate Inertial Response," *IEEE Transactions on Power Systems* 28, no. 3 (2013): 2283–2291, https://doi.org/10.1109/TPWRS.2012.2236365.
- 12. S. Morovati, S. M. Djouadi, M. Olama, et al., "Inertia Emulation Control Using Demand Response via 5G Communications," in 2021 IEEE 12th International Symposium on Power Electronics for Distributed Generation Systems (PEDG) (Chicago, IL: IEEE, 2021), 1–5, https://doi.org/10.1109/PEDG51384.2021.9494275.
- 13. J. Morren, D. Haan, W. H. Sjoerd, W. L. Kling, and J. A. Ferreira, "Wind Turbines Emulating Inertia and Supporting Primary Frequency Control," *IEEE Transactions on Power Systems* 21, no. 1 (2006): 433–434.
- 14. J. M. Mauricio, A. Marano, A. Gomez-Exposito, M. Ramos, and J. É. Luis, "Frequency Regulation Contribution Through Variable-Speed Wind Energy Conversion Systems," *IEEE Transactions on Power Systems* 24, no. 1 (2009): 173–180, https://doi.org/10.1109/TPWRS.2008.2009398.
- 15. K. V. Vidyanandan and N. Senroy, "Primary Frequency Regulation by Deloaded Wind Turbines Using Variable Droop," *IEEE Transactions on Power Systems* 28, no. 2 (2013): 837–846, https://doi.org/10.1109/TPWRS .2012.2208233.
- 16. A. Junyent-Ferr, Y. Pipelzadeh, and T. C. Green, "Blending HVDC-Link Energy Storage and Offshore Wind Turbine Inertia for Fast Frequency Response," *IEEE Transactions on Sustainable Energy* 6, no. 3 (2015): 1059–1066, https://doi.org/10.1109/TSTE.2014.2360147.
- 17. F. Wilches-Bernal, J. H. Chow, and J. J. Sanchez-Gasca, "A Fundamental Study of Applying Wind Turbines for Power System Frequency Control," *IEEE Transactions on Power Systems* 31, no. 2 (2016): 1496–1505, https://doi.org/10.1109/TPWRS.2015.2433932.
- 18. P.-K. Keung, P. Li, H. Banakar, and B. T. Ooi, "Kinetic Energy of Wind-Turbine Generators for System Frequency Support," *IEEE Transactions on Power Systems* 24, no. 1 (2009): 279–287.
- 19. L. Miao, J. Wen, H. Xie, C. Yue, and W.-J. Lee, "Coordinated Control Strategy of Wind Turbine Generator and Energy Storage Equipment for

- Frequency Support," *IEEE Transactions on Industry Applications* 51, no. 4 (2015): 2732–2742, https://doi.org/10.1109/TIA.2015.2394435.
- 20. S. Wang and K. Tomsovic, "A Novel Active Power Control Framework for Wind Turbine Generators to Improve Frequency Response," *IEEE Transactions on Power Systems* 33, no. 6 (2018): 6579–6589.
- 21. Y. Zhang, M. Olama, A. Melin, Y. Xue, S. Djouadi, and K. Tomsovic, "Synthesizing Distributed Energy Resources in Microgrids With Temporal Logic Specifications," in *IEEE International Symposium on Power Electronics for Distributed Generation Systems (PEDG)* (Charlotte, USA: IEEE, 2018), 1–7.
- 22. W. He, X. Yuan, and J. Hu, "Inertia Provision and Estimation of PLL-Based DFIG Wind Turbines," *IEEE Transactions on Power Systems* 32, no. 1 (2017): 510–521, https://doi.org/10.1109/TPWRS.2016.2556721.
- 23. L. Zhang, L. Harnefors, and H.-P. Nee, "Power-Synchronization Control of Grid-Connected Voltage-Source Converters," *IEEE Transactions on Power Systems* 25, no. 2 (2010): 809–820, https://doi.org/10.1109/TPWRS .2009.2032231.
- 24. W. Zhang, A. M. Cantarellas, J. Rocabert, A. Luna, and P. Rodriguez, "Synchronous Power Controller With Flexible Droop Characteristics for Renewable Power Generation Systems," *IEEE Transactions on Sustainable Energy* 7, no. 4 (2016): 1572–1582, https://doi.org/10.1109/TSTE .2016.2565059.
- 25. R. Bhana and T. J. Overbye, "The Commitment of Interruptible Load to Ensure Adequate System Primary Frequency Response," *IEEE Transactions on Power Systems* 31, no. 3 (2016): 2055–2063.
- 26. F. M. Uriarte, C. Smith, S. VanBroekhoven, and R. E. Hebner, "Microgrid Ramp Rates and the Inertial Stability Margin," *IEEE Transactions on Power Systems* 30, no. 6 (2015): 3209–3216.
- 27. W.-H. Chen, J. Yang, and S. Li, "Disturbance-Observer-Based Control and Related Methods—An Overview," *IEEE Transactions on Industrial Electronics* 63, no. 2 (2016): 1083–1095.
- 28. Y. Wei, G.-P. Liu, H. Jun, and F. Mengi, "Disturbance Attenuation and Rejection for Nonlinear Uncertain Switched Systems Subject to Input Saturation," *IEEE Access* 7, (2019): 58475–58483, https://doi.org/10.1109/ACCESS.2019.2914738.
- 29. Y. Huang and W. Xue, "Active Disturbance Rejection Control: Methodology and Theoretical Analysis," *ISA Transactions* 53, no. 4 (2014): 963–976.
- 30. H. Feng and B.-Z. Guo, "Active Disturbance Rejection Control: Old and New Results," *Annual Reviews in Control* 44 (2017): 238–248.
- 31. H. W. Knobloch, *Disturbance Attenuation for Uncertain Control Systems* (Switzerland: Springer, 2014), https://doi.org/10.1007/978-3-319-00957-5.
- 32. S. Prajna, A. Jadbabaie, and G. J. Pappas, "A Framework for Worst-Case and Stochastic Safety Verification Using Barrier Certificates," *IEEE Transactions on Automatic Control* 52, no. 8 (2007): 1415–1428.
- 33. R. E. Skelton, T. Iwasaki, and D. E. Grigoriadis, *A Unified Algebraic Approach to Control Design* (London: Tylor & Francis, 1997).
- 34. M. C. de Olivera, "A Robust Version of the Elimination Lemma," *IFAC World Comgress* 38, no. 12 (2005): 310–314.
- 35. H. T. M. Kussaba, J. Y. Ishihara, and R. A. Borges, "Uniform Versions of Finsler's Lemma," in 2015 54th IEEE Conference on Decision and Control (CDC) (Osaka, Japan: IEEE, 2015), 7292–7297, https://doi.org/10.1109/CDC.2015.7403370.
- 36. K. Gu, "An Integral Inequality Problem of Time-Delay Systems," in *IEEE Conference on Decision and Control (CDC)* (Sydney, NSW: IEEE, 2000), 2805–2810, https://doi.org/10.1109/CDC.2000.914233.
- 37. S. Morovati and H. Pulgar-Painemal, "Control Coordination Between DFIG-Based Wind Turbines and Synchronous Generators for Optimal

- Primary Frequency Response," in 52nd North American Power Symposium (NAPS) (Tempe, AZ: IEEE, 2021), 1–6, https://doi.org/10.1109/NAPS50074.2021.9449796.
- 38. Y. Zhang, K. Tomsovic, S. Djouadi, and H. Pulgar-Painemal, "Hybrid Controller for Wind Turbine Generators to Ensure Adequate Frequency Response in Power Networks," *IEEE Journal on Emerging and Selected Topics in Circuits and Systems* 7, no. 3 (2017): 359–370.
- 39. H. A. P. Painemal, Wind Farm Model for Power System Stability Analysis (Champaign, IL: Univ. of Illinois at Urbana-Champaign, 2010).
- 40. Y. Zhang, A. M. Melin, S. M. Djouadi, M. M. Olama, and K. Tomsovic, "Provision for Guaranteed Inertial Response in Diesel-Wind Systems via Model Reference Control," *IEEE Transactions on Power Systems* 33, no. 6 (2018): 6557–6568.
- 41. J. Zhen and D. Hertog, "Dick Computing the Maximum Volume Inscribed Ellipsoid of a Polytopic Projection," *INFORMS Journal on Computing* 30, no. 1 (2018): 31–42.
- 42. P. Finsler, "Uber das Vorkommen Definiter und Semidefiniter Formen in Scharen Quadratischer Formen," *Commentarii Mathematici Helvetici* 9 (1937): 188–192.
- 43. M. C. de Olivera and R. Skelton, "E Stability Tests for Constrained Linear Systems," in *Perspectives in Robust Control*. Lecture Notes in Control and Information Science, vol. 268 (NY: Springer-Verlag, 2001), 241–257.
- 44. S. M. Djouadi, "A Note on the Optimality of Balanced Truncation for a Class of Infinite Dimensional Systems," in *Proceedings of the American Control Conference (ACC)* (Sandiego, CA: IEEE, 2023), https://doi.org/10.23919/ACC55779.2023.10156457.
- 45. S. Morovati, Y. Zhang, S. M. Djouadi, K. Tomsovic, A. Wintenberg, and M. Olama, "Robust Output Feedback Control Design for Inertia Emulation by Wind Turbine Generators," *IEEE Transactions on Power Systems* 36, no. 6 (2021): 5056–5067, https://doi.org/10.1109/TPWRS.2021.3070276.
- 46. M. J. D. Hayes and D. John, "Maximum Area Ellipses Inscribing Specific Quadrilaterals," in *Proceedings of the 2016 CSME International Congress* (Kelowna, Canada: CCToMM, 2016).

Appendix A

A.1 | DFIG-Based WTG Model

The DFIG-based WTG is defined by the following set of differential-algebraic equations [39,40]:

$$\dot{\psi}_{qs} = \overline{\omega}(v_{qs} - R_s i_{qs} - \omega_s \psi_{ds}) \tag{A1}$$

$$\dot{\psi}_{ds} = \overline{\omega}(v_{ds} - R_s i_{qs} - \omega_s \psi_{qs}) \tag{A2}$$

$$\dot{\psi}_{ar} = \overline{\omega}[v_{ar} - R_r i_{ar} - (\omega_s - \omega_r)\psi_{dr}] \tag{A3}$$

$$\dot{\psi}_{dr} = \overline{\omega} [v_{dr} - R_r i_{dr} - (\omega_s - \omega_r) \psi_{qr}]$$
 (A4)

$$\dot{\omega}_r = (T_m - T_e)/(2H_T) \tag{A5}$$

$$\dot{\omega}_f^* = \omega_c(\omega_r^* - \omega_f^*) \tag{A6}$$

$$\dot{x}_1 = K_I^T(\omega_f^* - \omega_r + u) \tag{A7}$$

$$\dot{x}_2 = K_I^Q(Q_g^* - Q_g) \tag{A8}$$

$$\dot{x}_3 = K_I^C (i_{qr}^* - i_{qr}) \tag{A9}$$

$$\dot{x}_4 = K_I^C (i_{dr}^* - i_{dr}) \tag{A10}$$

$$0 = -\psi_{qs} + L_s i_{qs} + L_m i_{qr} \tag{A11}$$

$$0 = -\psi_{ds} + L_s i_{ds} + L_m i_{dr} \tag{A12}$$

$$0 = -\psi_{ar} + L_r i_{ar} + L_m i_{as} \tag{A13}$$

$$0 = -\psi_{dr} + L_r i_{dr} + L_m i_{ds} \tag{A14}$$

$$0 = P_g + (v_{qs}i_{qs} + v_{ds}i_{ds}) + (v_{qr}i_{qr} + v_{dr}i_{dr})$$
(A15)

$$0 = Q_g + (v_{qs}i_{qs} - v_{ds}i_{qs}) + (v_{qr}i_{dr} - v_{dr}i_{qr})$$
(A16)

$$0 = -v_{qr} + x_3 + K_P^C(i_{qr}^* - i_{qr}) +$$

$$(\omega_s - \omega_r) \left(\sigma L_r i_{dr} + \frac{\Psi_s L_m}{L_s}\right)$$
(A17)

$$0 = -v_{dr} + x_4 + K_p^C (i_{dr}^* - i_{dr}) - (\omega_s - \omega_r) \sigma L_r i_{qr}$$
 (A18)

where $\psi_{dr}, \psi_{qr}, \psi_{ds}, \psi_{qs}$ are the rotor and stator flux linkages in d, q axis, respectively. $\hat{i}_{dr}, i_{qr}, i_{ds}, i_{qr}$ are the instantenuous rotor and stator currents in d, q axis. $v_d r$, $v_q r$, $i_d s$ $i_q s$ are the instantaneous rotor and stator voltages in d, q axis. R_s and R_r are the stator and rotor resistances. $\overline{\omega}$, ω_s , ω_r , ω_c, ω_f^* are speed bases of WTG, synchronous angular speed, wind turbine angular speed, cutt-off frequency of low-pass filter and reference speed for WTG. K_I^Q , K_I^T , K_I^C , and K_P^C are integral gain of reactive power, torque, current controllers and proportional gain of current controller. L_r , L_s , L_m are rotor, stator, mutual inductances. $L_l r$ and L_{ls} are the rotor ans stator leakage inductions. Q_g and P_g are the reactive and active power of the WTG. σ is the leakage coefficient of induction machines. T_m is the mechanical torque and $T_e = \frac{L_m}{L} (\psi_{qs} i_{dr} - \psi_{ds} i_{qr})$. Equation (A1-A5) are the dynamics of the induction machine in the synchronous d-q reference frame. The dynamical model of the rotor side converter (RSC) control is given in (A6-A10). The algebraic relations of the flux linkages and electric power are expressed in (A17-A18). The loop of algebraic equations is closed by the algebraic relations in (A9) and (A10). The state variables x_1 , x_2 and x_3 , x_4 are related to the speed and the reactive power controllers of the WTG, respectively.

A.2 | SMA-Based Model Reduction Technique

The differential-algebraic model of WTG in (A1–A18) is linearized about the equilibrium point to give the state-space model. Let $x_{\omega} = [\psi_{as}, \psi_{ds}, \psi_{ar}, \psi_{dr}, \omega_r, \omega_r^*, x_1, x_2, x_3, x_4]^T$,

$$\begin{split} \Delta \dot{x}_{\omega} &= A_{sys} \Delta x_{\omega} + B_{sys} u \\ \Delta P_{e} &= C_{sys} \Delta x_{\omega} + D_{svs} u \end{split} \tag{A19}$$

Using the SMA-model reduction method, Equation (A19) will be reduced to a first order system, such that (A19) can be rearranged as

$$\begin{bmatrix} \Delta \dot{\omega}_r \\ \dot{z} \end{bmatrix} = \begin{bmatrix} A_{11} & A_{12} \\ A_{21} & A_{22} \end{bmatrix} \begin{bmatrix} \Delta \omega_r \\ z \end{bmatrix} + \begin{bmatrix} B_r \\ B_z \end{bmatrix} u$$

$$\Delta P_g = \begin{bmatrix} C_r & C_z \end{bmatrix} \begin{bmatrix} \Delta \omega_r \\ z \end{bmatrix} + D_{sys} u$$
(A20)

The most relevant dynamic is described by [39]

$$\Delta\dot{\omega}_r = A_{11}\Delta\omega_r + A_{12}z + B_ru \tag{A21}$$

The less relevant dynamics are

$$\dot{z} = A_{22}z + A_{21}\Delta\omega_r + B_z u \tag{A22}$$

z can be represented by the following expression

$$z(t) = e^{A_{22}(t-t_0)} z(t_0) + \int_{t_0}^t e^{A_{22}(t-\tau)} A_{21} \Delta \omega_r(\tau) d\tau$$

$$+ \int_{t_0}^t e^{A_{22}(t-\tau)} B_z u(\tau) d\tau$$
(A23)

The mode where $\Delta\omega_r$ has the highest participation would capture the relevant active power dynamics and is considered as the most relevant mode, and $\Delta\omega_r(\tau)=c_rv_re^{\lambda_r\tau}$ where λ_r is the most relevant mode, v_r is the corresponding eigenvector and c_r is a constant which depends on the initial state. Since the electrical dynamics related to A_{22} are faster than the electro-mechanical ones, the largest eigenvalue of A_{22} is much smaller than λ_r . Thus, the natural response will decay faster and can be omitted. So the first two terms in (A23) can be approximated by $(\lambda_r I - A_{22})^{-1}A_{21}\Delta\omega_r$ and the second integral by $M = (-A_{22})^{-1}B_z + \delta$. The response of the less relevant dynamics are expressed as $z \approx (\lambda_r I - A_{22})^{-1}A_{21}\Delta\omega_r + Mu$, and we get from (A20) and (A21)

$$\Delta \dot{\omega}_r = A_{rd} \Delta \omega_r + B_{rd} u$$

$$\Delta P_{\sigma} = C_{rd} \Delta \omega_r + D_{rd} u$$

with $A_{rd} = (A_{11} + A_{12}(\lambda_r I - A_{22})^{-1} A_{21}) B_{rd} = (A_{12}M + B_r), C_{rd} = (C_r + C_z(\lambda_r I - A_{22})^{-1} A_{21})$, and $D_{rd} = (C_z M + D_{sys})$ (see [35] for more details).

Appendix B

The computation of γ satisfying (21) is performed according to the following Lemmas

Lemma 3. ([33]). Let $M = M^T$ and $N = N^T > 0$. Then $\exists \gamma \in \mathbb{R}$, such that $M - \gamma N < 0$. In fact, such γ is given by

$$\gamma = \frac{\lambda_{\max}(M) + |\lambda_{\max}(M)|}{\lambda_{\min}(N)} + 1$$

where $\lambda_{max}(.)$ and $\lambda_{min}(.)$ denote the maximum and the minimum eigenvalues, respectively.

Remark 5. If the condition (19) is satisfied, then the existence of the controller K is ensured, and γ can be computed using Lemma 3, such that $\gamma = \frac{\lambda_{\max}(Q) + |\lambda_{\max}(Q)|}{\lambda_{\min}((PB_2)(PB_2)^*)} + 1, \text{ with } Q = A^TP + PA + \frac{1}{\eta}PB_1B_1^TP.$

Lemma 4. ([33]). For a matrix $B \in \mathbb{R}^{n \times m}$ with rank r, let $B^{\perp} \in \mathbb{R}^{(n-r) \times n}$ be any matrix such that $B^{\perp}B = 0$ and $B^{\perp}B^{\perp *} > 0$. The set of such matrices can be computed by $B^{\perp} = TU_2^*$, where T is an arbitrary non-singular matrix and U_2 is from the singular value decomposition $B = \begin{bmatrix} U_1 & U_2 \end{bmatrix} \begin{bmatrix} \sum_1 & 0 \\ 0 & 0 \end{bmatrix} \begin{bmatrix} V_1^* \\ V_2^* \end{bmatrix}$. Let $Q = Q^T \in \mathbb{R}^{n \times n}$ be given. Let (B_l, B_r) be any full rank factor of B that is, $B = B_l B_r$, and define $\Phi = (B_r B_r^*)^{-0.5} B^+$, where B^+ is the Moore-Pseudo inverse of B. Then, the following statements are equivalent:

- i. $\exists \gamma \text{ such that } \gamma BB^* Q > 0$.
- ii. The following condition holds: $B^{\perp}QB^{\perp *} < 0$,

and all scalars γ satisfying (i) are given by

$$\gamma > \gamma_{\min} = \lambda_{\max} [\Phi(Q - QB^{\perp*}(B^{\perp}QB^{\perp*})^{-1}B^{\perp}Q)\Phi^*]$$

Note that, for a nonsingular matrix $\Psi = \begin{bmatrix} \Phi \\ B^{\perp} \end{bmatrix}$, and by congruence transformation with Ψ , condition (i) is equivalent to $\begin{bmatrix} \gamma I - \Phi Q \Phi^* & -\Phi Q B^{\perp *} \\ -B^{\perp} Q \Phi^* & -B^{\perp} Q B^{\perp *} \end{bmatrix} > 0$. Using the Shur complement, we get $\gamma I - \Phi (Q - Q B^{\perp *} (B^{\perp} Q B^{\perp *})^{-1} B^{\perp} Q) \Phi^* > 0$, which results in the computation of γ .

Remark 6. If the condition (18) is satisfied, then the existence of the controller K is guaranteed and γ can be computed using Lemma 4 by considering $B = (PB_2)$ and $Q = A^TP + PA + \frac{1}{n}PB_1B_1^TP$.